Journal of Colloid and Interface Science **218,** 309–323 (1999)
Article ID jcis.1999.6426, available online at http://www.idealibrary.com on IDEAL®

Modeling Draining Flow in Mobile and Immobile Soap Films

L. W. Schwartz[1] and R. V. Roy

Departments of Mechanical Engineering and Mathematical Sciences, The University of Delaware, Newark, Delaware 19716

Received March 25, 1999; accepted July 12, 1999

A mathematical model is constructed to describe the two-dimensional flow in a vertical soap film that is draining under gravity. An asymptotic analysis is employed that uses the long-wave or "lubrication" approximation. The modeling results in three coupled partial differential equations that include a number of dimensionless input parameters. The equations are solved numerically. The three functions calculated, as they vary in space and time, are the film thickness, the surface concentration of an assumed insoluble surfactant, and the slip or surface velocity. The film is assumed to be supported by "wire frame" elements at both the top and the bottom; thus the liquid area and the total surfactant are conserved in the simulation. A two-term "disjoining" pressure is included in the model that allows the development of thin, stable, i.e., "black," films. While the model uses a simplified picture of the relevant physics, it appears to capture observed soap film shape evolution over a large range of surfactant concentrations. The model predicts that, depending on the amount of surfactant that is present, the film profile will pass through several distinct phases. These are (i) rapid initial draining with surfactant transport, (ii) slower draining with an almost immobile interface due to the surface tension gradient effect, and (iii) eventual formation of black spots at various locations on the film. This work is relevant to basic questions concerning surfactant efficacy, as well as to specific questions concerning film and foam draining due to gravity. Prospects for extension to three-dimensional soap film flows are also considered.

Key Words: **soap films; draining; surfactant; mathematical model; numerical simulation; surface tension; disjoining pressure; fluid mechanics.**

1. INTRODUCTION

The now classical study of Mysels *et al.* (1) gives a comprehensive experimental description of the draining and thinning of soap films. Many other workers, both before and since, have reported observations of soap films and bubbles, starting perhaps with the early studies of Isaac Newton (2). Interferometric measurements are straightforward and can yield film thickness profiles to high accuracy as they evolve in time. Interfacial films with surfactant can be considered as the basic building blocks for foams and high-quality emulsions. Fundamental issues dealing with surfactant effects and the flow of multiphase mixtures, including emulsions, are relevant to a number of consumer products including prepared foods, the manufacture of solid foams, processing issues in the petrochemical industry, and the biological/life sciences (3, 4, 5). Recent mathematical models that seek to predict the lifetime of foams require, as a starting point, information concerning the behavior of the films that form the walls of the foam cells (6, 7). Motion within films and foams is determined primarily by the action of viscous, surface tension, gravitational, and Marangoni, i.e., surface-tension-gradient, forces. These cause films to drain and thin, including motion into the interstitial junctures, the so-called Plateau borders, where three or more soap films meet.

The experimental work in Mysels *et al.* (1) used soap films attached to wire frames. Their results included a number of interesting features:

(i) For large surfactant concentration, film boundaries become immobile. These immobile films are concave-in and have the form of vertical, downward opening parabolas. They are several microns thick on average and drain relatively slowly. Drawings of the experimental results are shown for times as long as 1 h.

(ii) For relatively small surfactant concentration the film boundaries are mobile. Mobile films drain more quickly and are concave-out, termed "hollow ground" by Mysels *et al.* No theory is given by them, but it can be surmised that insufficient surface tension gradient develops to immobilize the free surface. Films thin to less than a micron in under 1 min.

(iii) In both cases, the film is suspended at the top from a very thin film, termed "black film." The length of the black film region grows with time.

When the wire frames had vertical sides, the flow patterns were more complicated. There was sideways flow into the Plateau borders when side frame elements were present. This flow into borders is termed by them "marginal regeneration." Another fascinating observation is that thin "black" spots form near the bottom of a vertical film and rise until they reach a level where the local film thickness is equal to the spot thickness. The spot movement is somewhat chaotic, giving rise to the phrase "turbulence in soap films." An analogy has often been cited to bubbles rising in a liquid, resulting from the action of buoyancy. In the buoyant analogy the effective density is the thick-

[1] To whom correspondence should be addressed.

0021-9797/99 $30.00

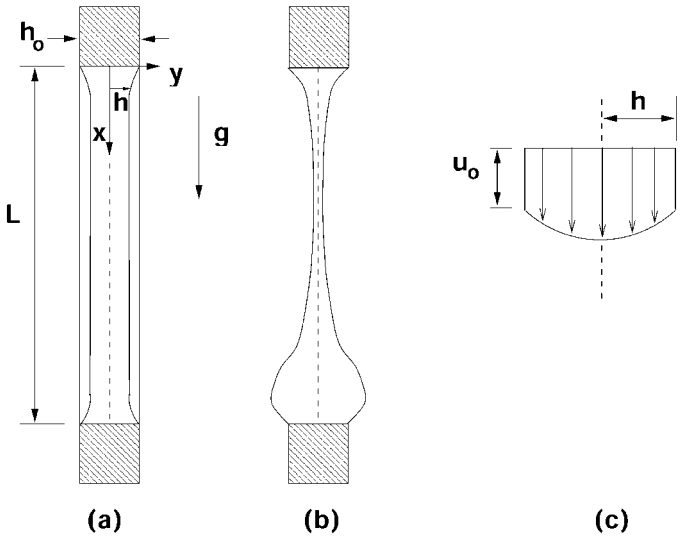

FIG. 1. Definition sketch for (a) the initial state of a soap film held vertically between upper and lower supports for two different initial profile shapes. (b) Sketch of the soap film at a later time showing gravity drainage. (c) The downward velocity profile is a linear combination of a slug flow at the interface slip velocity u_0 and a parabolic shear flow.

ness of the liquid film. The two-dimensional draining patterns that they obtained were realized by using circular cylindrical films without sidewall boundaries. These cylindrical films were suspended from a horizontal wire hoop whose radius was, of course, much larger than the film thickness dimensions.

This report presents a mathematical model for the time-dependent evolution and drainage, under gravity, of thin liquid films with surfactant. Our goal is to produce a model of minimum complexity while still capturing the important features of the process, including the transition from an essentially mobile film to an immobile or "hardened" one as time proceeds. We will make a number of simplifying assumptions involving film geometry and the nature of the liquid and surfactant transport processes. The simplifications serve a dual purpose; they make the model easier to solve and also aid in identifying the dominant mechanisms responsible for observed behavior.

In the model, the film is exposed to the atmosphere on both sides, and bilateral symmetry about a vertical centerline is assumed. Definition sketches are given in Fig. 1. The film shapes at the start of the simulation and at a later time, after a degree of drainage has occurred, are shown schematically in Figs. 1a and 1b. The origin of coordinates is taken at the center of the upper support. Two possible initial conditions are given in Fig. 1a. A representative velocity profile is illustrated in Fig. 1c. As will be demonstrated, it is formed from a superposition of extensional and shear flow components.

The simplest assumption when a surfactant is present is that the liquid–air interface is "hard" or immobile. In that case, under the lubrication approximation, drainage, or other flow problems, are effectively identical to flow on a no-slip substrate. This results in a great simplication and only a single evolution equation must be solved. The simplest extension of the present work to unsteady three-dimensional problems is to retain the hardened-surface assumption.

Schwartz and Princen (8) used the hardened-film approximation to treat certain aspects of flow in free films by extending the asymptotic analysis of Landau and Levich (LL, see Levich (9)), who predicted the thickness of a liquid film applied to a solid substrate as it is slowly removed from a bath. By assuming that gas–liquid interfaces within a foam contain sufficient surfactant to become immobile, Schwartz and Princen showed that the LL analysis could be used locally to predict the flow rate to and from films and Plateau borders within a foam that is in periodic deformation. The radius of curvature of the borders can, in the limiting case of very slow motion, be calculated if the bubble size and gas fraction are both given. In that work unsteady motions are treated as a slowly varying succession of steady-state flows.

Rather than use quasi-static analytical approximation, here unsteady evolution equations are derived and solved numerically. A simplified form of the present technique was used in another time-dependent problem, the leveling of ripples in a thin coating layer on a flat substrate in the absence of gravity (10, 11). That problem is also a thin film flow, with a mobile free surface, surfactant transport, and surface-tension-gradient effect. Because of the no-slip condition on the substrate, the flow is essentially shear-dominated for all time. The interface velocity is given explicitly in terms of the other unknowns; thus only two coupled equations, for the layer thickness $h(x, t)$ and the surfactant concentration $\Gamma(x, t)$, respectively, need to be solved. The model showed that, for large surfactant concentration, the surface becomes hardened. The presence of surfactant generally retards leveling. However, in the hardened state, leveling can be more rapid than for lower concentrations for which the surface remains mobile. This surprising conclusion was verified by comparing a linearized closed-form solution, valid for ripples of small initial amplitude (10), with lubrication-model numerical solutions as well as with finite-element solution of the full creeping-motion equations (11).

Following Frumkin (12) and Deryaguin (13), the present model uses an additional or "disjoining" pressure Π to account for the interaction of the surface layers in the two-sided free film. The particular functional forms for $\Pi(h)$ used here have stable energy minima when the film thickness takes on a particular small value. This stable thickness is identified with the occurrence of "black" film. A disjoining pressure function exhibiting an energy minimum can also be used to model the energetics of a finite equilibrium contact angle at a three-phase point where gas and liquid meet on a flat solid substrate (14). Disjoining pressure terms of various forms have been included in evolution equations for the motion of two-dimensional liquid layers on solid surfaces by a number of authors (15–18). Recently evolution equations, with disjoining effect, have been formulated and solved in models for three-dimensional droplet

motions on chemically heterogeneous substrates (19, 20). General methods for three-dimensional unsteady calculations of thin-film flows on solid substrates are discussed in (21). Two-dimensional flow models for free films with surface slip have also appeared, either without surfactant (22) or with surfactant effects included (23–25). As in the present work, these models employed the lubrication approximation. A recent modeling study of a two-dimensional deforming droplet with surfactant uses the unapproximated creeping-motion equations (26).

The dimensionless problem for two-dimensional flow is derived in the following section by a systematic expansion of the governing equations in the thin film limit. This results in a coupled set of equations for the film profile, the surface slip velocity and the surfactant concentration, as well as the required boundary and initial conditions. The derivation assumes an intermediate situation where extensional and shear flow contributions to the pressure gradient are of equal importance. The model equations remain valid in the two limiting cases where one or the other of the two contributions is missing. The shear stresses on the film–air interface are caused by the nonuniform distribution of surfactant there.

Sample calculations are presented in Section 3. A number of the features observed experimentally by Mysels *et al.* (1) are reproduced by the simulation. Several initial configurations are treated. In each case the surfactant concentration is initially uniform. The simulations show how the surfactant is transported, in an efficient way, to those locations on the interface where it is needed to support the weight of the film. The model appears able to identify the critical surfactant concentration necessary to make the interface immobile everywhere so that drainage is maximally retarded.

The concluding section discusses extensions of the present work. These include relaxation of some of the assumptions in the model and the prospects for three-dimensional simulation.

2. THE MATHEMATICAL MODEL FOR DRAINING SOAP FILMS

We derive a mathematical model for the draining flow in mobile and immobile soap films. The liquid within soap films evolves under the combination of gravity forces, viscous forces, surface tension forces, disjoining pressure, and Marangoni forces due to the presence of surfactant. Surfactant transport on the film free surface is in part due to differentials of surface tension which can drive fluid motion. We consider a vertical two-dimensional soap film supported at the top and bottom by wires. The liquid–air interfaces are located at $y = \pm h(x, t)$; i.e., we assume the film to be left–right symmetric with respect to the centerline $y = 0$, and we consider, henceforth, only the half-film $h \geq 0$. Within the realm of lubrication theory, we expect to find three partial differential equations governing the film (half) thickness $h(x, t)$, the surface slip velocity $u_0(x, t)$, and the surfactant concentration $\Gamma(x, t)$.

We assume that the regime of the flow is characterized by a very small value of the Reynolds number Re, so that the inertia term $\rho D\mathbf{u}/Dt$ can be neglected in comparison to the viscous force per unit volume of the fluid. That is, $Vh_0/\nu \ll 1$ is assumed, where V is a typical fluid velocity, h_0 is a reference film thickness, and $\nu = \mu/\rho$ is the kinematic viscosity of the fluid. Therefore, assuming constant viscosity and constant density, the governing equations for the fluid velocity $\mathbf{u} = (u, v)$ and pressure p are given by the mass conservation and the momentum conservation equations (continuity and Stokes equations),

$$\frac{\partial u}{\partial x} + \frac{\partial v}{\partial y} = 0 \qquad [2.1]$$

$$-\frac{\partial p}{\partial x} + \mu\left(\frac{\partial^2 u}{\partial x^2} + \frac{\partial^2 u}{\partial y^2}\right) + \rho g = 0 \qquad [2.2a]$$

$$-\frac{\partial p}{\partial y} + \mu\left(\frac{\partial^2 v}{\partial x^2} + \frac{\partial^2 v}{\partial y^2}\right) = 0, \qquad [2.2b]$$

which hold within the fluid half-layer $0 \leq y \leq h(x, t)$.

Corresponding boundary conditions are reflection symmetry conditions at $y = 0$, that is,

$$v = 0, \quad \frac{\partial u}{\partial y} = 0, \qquad [2.3]$$

and the kinematic condition at the free surface $y = h$,

$$h_t = v - uh_x, \qquad [2.4]$$

using the subscript notation $h_t = \partial h/\partial t$ and $h_x = \partial h/\partial x$. The shear stress $\tau(x, t)$ at the free surface $y = h$ satisfies

$$\mu(1 - h_x^2)\left(\frac{\partial u}{\partial y} + \frac{\partial v}{\partial x}\right) + 2\mu h_x\left(\frac{\partial v}{\partial y} - \frac{\partial u}{\partial x}\right) = \tau(x, t). \qquad [2.5]$$

Values of the surface shear stress will be related to the concentration of surfactant. The normal stress condition at the free surface $y = h$ is

$$-p + \frac{2\mu}{1 + h_x^2}\left\{h_x^2\frac{\partial u}{\partial x} - h_x\left(\frac{\partial u}{\partial y} + \frac{\partial v}{\partial x}\right) + \frac{\partial v}{\partial y}\right\} = -p^{(s)}, \qquad [2.6]$$

where $p^{(s)}$ is the pressure on the liquid side of the free surface. It will subsequently be assumed to be the sum of capillary and "disjoining" components.

An integral expression of conservation of mass is

$$\frac{\partial h}{\partial t} = -\frac{\partial Q}{\partial x} = -\frac{\partial}{\partial x}\int_0^h u(t, x, y)dy, \qquad [2.7]$$

where Q is the volumetric flow rate. Thus, determination of a small-slope evolution equation for $h(x, t)$ amounts to finding an approximation for Q.

2.1. Scaling and Nondimensionalization

If L is a characteristic length scale along the downward direction (as in Fig. 1), assuming a thin geometry, a typical scale of width is

$$h_0 = \epsilon L,$$

where $\epsilon \ll 1$. The dominant downward component of the flow field is subdivided into a purely extensional or "slug" flow contribution $u_0 \equiv u_0(x, t)$ and a shear component $u_1 = u_1(x, y, t)$ that satisfies $u_1 = 0$ at $y = h$. Thus u_1 satisfies the no-slip condition at the free surface. We consider an intermediate regime where the two flow contributions have a comparable dynamic effect on the downward pressure gradient. The assumed scaling is

$$p_{0x} \sim \mu u_{0xx} \sim \mu u_{1yy}.$$

The velocity scales are thus related according to

$$U_1 \sim \epsilon^2 U_0$$

for the extensional scale U_0 and the shear scale U_1. Furthermore the pressure scale is $P = \mu U_0/L$. Finally, the scale for the transverse velocity, according to the continuity equation, $v_y \sim u_{0x}$, is given by

$$V = \epsilon U_0.$$

We nondimensionalize the governing equations by introducing the nondimensional variables $x' = x/L$, $y' = y/(\epsilon L)$, $h' = h/(\epsilon L)$, $u_0' = u_0/U_0$, $u_1' = u_1/U_1$, $v' = v/V$, $p' = p/P$, $p^{(s)'} = p^{(s)}/P$, $\tau' = \tau/(\epsilon\mu U_0/L)$. We then obtain the nondimensional equations of motion and boundary conditions, dropping all primes for dimensionless variables,

$$u_{0x} + \epsilon^2 u_{1x} + v_y = 0 \qquad [2.8]$$

$$-p_x + u_{0xx} + \epsilon^2 u_{1xx} + u_{1yy} + Z = 0 \qquad [2.9]$$

$$-p_y + \epsilon^2 v_{xx} + v_{yy} = 0, \qquad [2.10]$$

where the dimensionless parameter

$$Z \equiv \rho g L^2/\mu U_0 = \frac{(\rho g L^2/\sigma)}{(\mu U_0/\sigma)}$$

is seen to be the ratio of Bond number over capillary number, as usually defined, and is assumed $\mathbb{O}(\epsilon^0)$. Here, σ is surface tension. The boundary conditions now read

$$v = 0, \quad u_{1y} = 0 \qquad [2.11]$$

on $y = 0$, and

$$(1 - \epsilon^2 h_x^2)(u_{1y} + v_x) + 2h_x(v_y - u_{0x} - \epsilon^2 u_{1x}) = \tau(x, t), \qquad [2.12]$$

$$-p + \frac{2}{1 + \epsilon^2 h_x^2}\{\epsilon^2 h_x^2(u_{0x} + \epsilon^2 u_{1x}) - \epsilon^2 h_x(u_{1y} + v_x) + v_y\} = -p^{(s)} \qquad [2.13]$$

on $y = h$.

2.2. Lubrication Model

We expand each unknown u_1, v, p in a power series in ϵ, assuming $\epsilon = h_0/L$ is a small number. Recall also that the "slip velocity" u_0 is also unknown.

$$u_1 \equiv u_1(x, t; \epsilon) = u_1^{(0)} + \epsilon^2 u_1^{(1)} + \cdots$$

$$v \equiv v(x, t; \epsilon) = v_0 + \epsilon^2 v_1 + \cdots$$

$$p \equiv p(x, t; \epsilon) = p_0 + \epsilon^2 p_1 + \cdots$$

At leading order, from (2.8), we first obtain $v_{0y} = -u_{0x}$ leading to

$$v_0 = -u_{0x} y$$

since $u_0 \equiv u_0(t, x)$ and $v_0 = 0$ at $y = 0$. Next we obtain p_0 from $p_{0y} = v_{0yy}$ and boundary condition $p_0 = 2v_{0y} + p^{(s)}$. With $v_{0yy} = 0$, we have $p_0 = p_0\ (y = h)$, independent of y:

$$p_0 = 2v_{0y} + p^{(s)}.$$

We can now find $u_{1y}^{(0)}$ by integration of $u_{1yy}^{(0)} = p_{0x} - u_{0xx} - Z$ from [2.9], yielding

$$u_{1y}^{(0)} = (p_{0x} - u_{0xx} - Z)y = -(3u_{0xx} - p^{(s)} + Z)y, \qquad [2.14]$$

where we have imposed the zero-shear condition $u_{1y}^{(0)} = 0$ at $y = 0$. The shear stress condition on the free surface [2.12] can now be imposed to yield an equation for the slip velocity u_0,

$$\tau = -4(hu_{0x})_x - h(-p^{(s)} + Z), \qquad [2.15]$$

which in dimensional variables becomes

$$\tau(x, t) = -h(-p_x^{(s)} + \rho g) - 4\mu(hu_{0x})_x. \qquad [2.16]$$

Finally one additional integration of [2.14] yields the shear velocity at leading order

$$u_1^{(0)} = -\tfrac{1}{2}(3u_{0xx} - p_x^{(s)} + Z)(y^2 - h^2). \qquad [2.17]$$

The evolution equation for h is then obtained from the expression of the downward velocity $u_0 + \epsilon^2 u_1^{(0)}$,

$$h_t = -(Q_0 + \epsilon^2 Q_1)_x, \quad Q_0 = u_0 h,$$
$$Q_1 = \tfrac{1}{3}h^3(3u_{0xx} - p_x^{(s)} + Z)$$

or, in dimensional variables,

$$h_t = -\left(u_0 h + h^3 u_{0xx} + \frac{\rho g}{3\mu} h^3 - \frac{h^3}{3\mu} p_x^{(s)}\right)_x. \qquad [2.18]$$

The evolution equation is completed by specifying the pressure at the free surface. Assuming constant atmospheric pressure outside the film, which may be taken equal to zero without loss of generality since only pressure differences drive the flow, the surface pressure, in dimensional units, is composed of capillary and disjoining components,

$$p^{(s)} = -\sigma\kappa - \Pi \approx -\sigma h_{xx} - \Pi. \qquad [2.19]$$

The surface curvature $\kappa = h_{xx}/(1 + h_x^2)^{3/2}$ has been approximated to consistent order. Since h_x is order ϵ the error in this curvature approximation is proportional to ϵ^2. The disjoining pressure is given by the two-term model

$$\Pi = A\left[\left(\frac{h^*}{h}\right)^n - \left(\frac{h^*}{h}\right)^m\right]. \qquad [2.20]$$

A and the exponents n and m are positive constants with $n > m > 1$. Note that the constant A has the dimensions of pressure. Since, for the present problem, the principal interactive force leading to disjoining effects is the mutual interaction between surfactant molecules on the opposing free surfaces, a more detailed model could have $A = A(\Gamma)$, where Γ is the local surfactant concentration.

Associated with the disjoining pressure is a local disjoining energy density

$$e^{(d)}(h) = -\int_{h^*}^{h} \Pi(h')dh'. \qquad [2.21]$$

Evidently $\Pi = -de^{(d)}/dh = 0$ at $h = h^*$; thus the model function [2.21] produces a single stable energy minimum at a (nominally thin) film thickness value $h = h^*$ and an attractive force at larger h values that decreases with increasing h. The shape of the "energy well" at h^* is determined by the constant A and the choice of exponents (n, m). Other disjoining pressure laws of the form $\Pi(h)$ that have a single energy minimum, such as those arising from a balance of Van der Waals and electrostatic repulsion, for example, can be approximated by choosing suitable values for these constants. The results presented here use the exponent pair $(n, m) = (4, 3)$. This choice and other choices have been used in the literature (16, 18, 19). Disjoining pressure issues are discussed further in Section 4.

Because the disjoining pressure is taken to depend only on the local interfacial separation $2h$, the validity of an expression such as [2.21] also requires the small-slope approximation. Disjoining pressure is relevant to very thin films, on the order of 100 nm total thickness or smaller. These very thin, or "black" films resist further thinning because of electrostatic repulsion between symmetrically placed surfactant molecules on the opposing liquid–gas interfaces. Black regions commonly occur in draining water–soap films (1).

2.3. Surfactant Effects

If the surface were uniformly "hard," u_0 would be identically zero and Eqs. [2.18] to [2.20] would suffice to determine the evolution of the film profile. The determination of the slip velocity u_0, in the general case, requires the solution of two additional equations. Surface tension gradients arise to help support the weight of the liquid film; thus the concentration of surfactant Γ must be monitored. A convection–diffusion evolution equation for an insoluble surfactant, for a film of small slope, is

$$\Gamma_t = -(u_0\Gamma)_x + D\Gamma_{xx}. \qquad [2.22]$$

Note that the first term on the right contains both a convection change $-u_0\Gamma_x$ as well as a reduction in concentration due to stretching $-\Gamma u_{0x}$. D is an assumed-constant Fickian diffusion coefficient. Note that, because [2.22] is linear in Γ, the form of this equation is independent of the units in which Γ is measured.

A relation $\sigma(\Gamma)$ is also required. The simplest form, valid for small changes in σ, is

$$\sigma = \sigma_0 - K(\Gamma - \Gamma_0), \qquad [2.23]$$

where K is a constant and the zero subscripts refer to the initial values of these quantities at the start of the motion. They will subsequently be used as reference quantities.

The surface shear stress in [2.16] is equal simply to the surface gradient of σ. For small slope, $\tau \approx \sigma_x = -K\Gamma_x$ using [2.23]. Equation [2.16] may then be written as

$$4\mu(hu_{0x})_x = K\Gamma_x - \rho gh - h(\sigma h_{xxx} + \Pi_x). \quad [2.24]$$

Equation [2.24] may be recognized as a local force balance on a film element of thickness h and length dx. The left side includes a factor of 4μ, the so-called "Trouton" viscosity for a thin falling film in pure extensional flow (27). Recently finite-element calculations for a long-thin falling viscous drop under the influence of gravity only, but with the use of unapproximated Stokes-flow equations [2.1, 2.2], have been performed (28). They confirm the validity of the approximation [2.24] in regions where the drop profile is thin, for that special case.

The condition [2.24] is equivalent to the assumption that elemental vertical forces are in exact balance. This is the usual Stokes creeping-motion assumption that the Reynolds number is sufficiently small that the acceleration or inertia terms in the governing equations can be neglected. Thus the time scale for film motion is much longer than the time required for the speed to equilibrate at its quasi-static value.

When Eqs. [2.18] and [2.19] are combined, the h evolution equation becomes

$$h_t = -(u_0 h + h^3 u_{0xx})_x - \frac{\rho g}{3\mu}(h^3)_x - \frac{\sigma_0}{3\mu}(h^3 h_{xxx})_x - \frac{1}{3\mu}(h^3\Pi_x)_x. \quad [2.25]$$

Equations [2.22], [2.24], and [2.25] form a complete set. Henceforth σ will be replaced by σ_0, as has been done in [2.25], implying that the fractional change in σ during a given simulation is small. This is also consistent with the linear law [2.23] used for $\sigma(\Gamma)$.

The problem has been formulated under the assumption that the elongational and shear components of the flow are of comparable importance. As will be demonstrated, when sufficient surfactant is present, the film will quickly "lock in" to a regime characterized by a no-slip interface with $u_0 \approx 0$ uniformly in x. Once this happens the forces on the right side of [2.24] will balance and only the film thickness evolution equation [2.25], with negligible u_0 terms, essentially determines the subsequent motion. The problem is then formally identical to two-dimensional thin film flow on a vertical wall, a problem that has been extensively studied (29). Conversely, for no or very small surfactant concentration, u_0 will be dominant for all time. Because the shear terms leading to Q_1 are formally two orders smaller in ϵ, they will be quite negligible for $\epsilon \ll 1$; then the evolution will be governed by the coupled solution of the simplified h equation

$$h_t \approx -(u_0 h)_x \quad [2.25a]$$

and Eq. [2.24] with the $K\Gamma_x$ term ignored. This latter limit corresponds essentially to cases treated by Stokes *et al.* (28). In the general case the solution will evolve in time from initially elongational to shear-dominated flow. Because validity has been established assuming that the two effects are comparable and because the model is valid in each limiting case, it is reasonable to infer that the model possesses uniform asymptotic validity for the entire range of temporal evolutions, when ϵ is small.

It can also be noted that the u_{0xx} term in [2.25] should have only a small relative effect for all times and can reasonably be discarded. When u_0 is important, this second-derivative term is formally $O(\epsilon^2)$ smaller than the u_0 term. It is also clearly unimportant when the flow is shear dominated. It will be omitted below, as a further model simplification. Some of the calculations given in Section 3 were repeated with this term retained, confirming that the term was indeed quite negligible.

2.4. The Full Problem in Dimensionless Form

The problem is completed by specifying the boundaries of the flow domain and the conditions there. Soap film experiments can be performed with a wire frame partially removed from a bath, in which case the film joins a static capillary–gravity meniscus at the bottom. They can also be performed using a full frame that includes a bottom boundary, with no bath. The latter case appears simpler and conservation of surfactant and liquid volume can also be enforced most simply. Thus we choose the latter model. Some recent work (30, 31) has considered drainage into a bath for an assumed tangentially immobile, i.e., a fully "hardened," film. When the film is assumed to be immobile, surfactant transport does not appear in the mathematical model and has no effect on the flow.

The time rate of change of the total surfactant is

$$\frac{d}{dt}\int_0^L \Gamma dx = -[u_0\Gamma|_L - u_0\Gamma|_0] + D[\Gamma_x(L) - \Gamma_x(0)] \quad [2.26]$$

from [2.22]. Thus conservation of surfactant is ensured if

$$u_0(0, t) = u_0(L, t) = 0 \quad [2.27a]$$

and

$$\Gamma_x(0, t) = \Gamma_x(L, t) = 0. \quad [2.27b]$$

If the ends of the film are fixed at the "edges" of the frame wires, as in Fig. 1, then

$$h(0, t) = h(L, t) = h_0, \quad [2.27c]$$

and, since the frame is impermeable,

$$Q(0, t) = Q(L, t) = 0, \qquad [2.27d]$$

where Q is given in [2.7]. Since the h equation [2.25] is fourth-order in space while the Γ and u_0 equations [2.22, 2.24] are each second-order, this is the correct number of boundary conditions. All that remains is to specify the initial fields $h(x, 0)$ and $\Gamma(x, 0)$. Note that the elliptic equation [2.24] for u_0 neither requires nor accepts an initial condition on u_0.

The problem is nondimensionalized as before, using, for film thickness dimensions,

$$h = h_0\tilde{h}, \qquad [2.28a]$$

and, for substrate coordinates,

$$x = L\tilde{x} \qquad [2.28b]$$

with

$$\epsilon = \frac{h_0}{L} \qquad [2.28c]$$

with h_0 and L as shown in Fig. 1. The reference time is defined by

$$t = T^*\tilde{t}, \quad T^* = \frac{3\mu L^4}{\sigma_0 h_0^3}. \qquad [2.28d]$$

Using this time scale sets the coefficient of the surface tension term in [2.25] equal to one. We also define the Bond number

$$B_0 = \frac{\rho g L^2}{\sigma_0}, \qquad [2.28e]$$

and, for convenience, a modified number

$$B_1 = B_0/\epsilon. \qquad [2.28f]$$

A dimensionless disjoining coefficient is formed as

$$\tilde{A} = \frac{A}{\epsilon^2(\sigma_0/h_0)}. \qquad [2.28g]$$

Similarly, the dimensionless diffusion coefficient and surface speed are formed using L and T^*,

$$\tilde{D} = \frac{D}{L^2/T^*}, \qquad [2.28h]$$

and

$$u_0 = (L/T^*)\tilde{U}. \qquad [2.28i]$$

The surfactant concentration is rescaled as

$$G = \frac{K}{\sigma_0\epsilon^2}\Gamma. \qquad [2.28j]$$

The disjoining pressure function is, without the A,

$$\tilde{\Pi} = \left(\frac{\tilde{h}^*}{\tilde{h}}\right)^n - \left(\frac{\tilde{h}^*}{\tilde{h}}\right)^m. \qquad [2.28k]$$

Finally, for convenience, we define

$$C = \frac{3}{4\epsilon^2}. \qquad [2.28l]$$

The differential equations, written in dimensionless form, with tildes omitted, are

$$h_t = -[Uh + h^3(B_1 + h_{xxx} + A\Pi_x)]_x, \qquad [2.29a]$$

$$G_t = -(UG)_x + DG_{xx}, \qquad [2.29b]$$

$$(hU_x)_x = C[G_x - h(B_1 + h_{xxx} + A\Pi_x)]. \qquad [2.29c]$$

Note the similar grouping of pressure gradient terms in [2.29a, 2.29c].

The boundary conditions are given below. The top and bottom frame support is the film thickness reference quantity; thus

$$h(0, t) = h(1, t) = 1. \qquad [2.30a]$$

At the ends, the conditions of no flow and no surfactant flux become

$$Q(0, t) = Q(1, t) = U(0, t) = U(1, t) = G_x(0, t) = G_x(1, t) = 0. \qquad [2.30b]$$

The initial conditions are

$$h(x, 0) = H(x), \quad G(x, 0) = G_0. \qquad [2.30c]$$

The initial film is prescribed by the function $H(x)$. Note that the constant K in [2.23] only appears in the defining group for G in [2.28j]. We will consider only an initially uniformly distributed surfactant; thus only the initial value G_0 needs to be specified in [2.30c]. Its value will be determined from the calculations; it will appear that a more or less well-defined

critical value exists, depending on the liquid area (or weight) that requires support. Either sufficient surfactant is present, actually the potential to support weight by developed surface tension gradients, or not. Weight support is the necessary ingredient for surface immobility. The magnitude of G_0 that will cause significant retardation of drainage can be estimated using [2.28j]. When the surface shear stress is comparable in magnitude to the local film weight per unit length, one obtains the scaling $\rho g h_0 \sim \sigma_x \sim K\Gamma_0/L$. Hence $G_0 \sim (\rho g L^2/\sigma_0)(L/h_0) = B_0/\epsilon$. Thus, for strong retardation, one expects G_0 to be of the same magnitude as B_1.

3. SAMPLE CALCULATIONS

The system of three coupled partial differential equations [2.29] has been solved using finite-difference methods. The scheme may be termed partially implicit in time. The nonlinear prefactors in the equations are evaluated using known values from the previous time level. In the numerical scheme the time step is adjustable and its value, at any stage in the calculation, is set by requiring that the maximum change in any film thickness value h is less than some preassigned global maximum. Convergence of the solution in both space and time has been verified, to graphical accuracy, for the results given here.

Certain physical parameters are well known to us while others are less well known. The length between supports L is 1 cm or more while h_0 depends, presumably, on the shape of the supports and could be, say, 0.005 cm = 50 μm. Other known parameters, in cgs units for water, are $\rho = 1$ gm/cm^3, $\sigma = 72$ dyne/cm (which could be reduced somewhat because of the presence of surfactant), and $\mu = 0.01$ poise. The viscosity could be very much higher for other liquids. If h^* is identified as (one-half) the black film thickness for aqueous solutions with certain surfactants, its value lies in the range 5–20 nm (1). For the largest value in this range, the ratio h^*/h_0 is 4 (10^{-4}); it is unlikely that we can calculate using such small values. Trends should be apparent for values of this ratio that are larger by a factor of 10 or 100. The diffusion constant D and the disjoining strength parameter A are taken to be constant. In a more complete model the latter, and perhaps the former, can be functions of concentration as well as the nature of the surfactant.

For the computation we assume a film length $L = 1$ cm and use the input dimensionless parameters formed from the physical values given:

$$\epsilon = h_0/L_0 = 0.005, \quad B_1 = 2725, \quad C = \frac{3}{4\epsilon^2} = 30{,}000.$$

The characteristic time is

$$T^* = 3333 \text{ s} = 0.93 \text{ h}.$$

The dimensionless disjoining constant and "black film" thickness are taken to be

$$A = 10, \quad h^* = 0.05,$$

respectively. The initial value of surfactant concentration is $G_0 = 500$. The disjoining exponent pair used is $(n, m) = (4, 3)$. For the results given here, the dimensionless diffusion constant has the value $D = 200$, a relatively small value. Much larger values of D can substantially reduce the development of Marangoni shear stresses on the interface, leading to more rapid draining.

Apart from the frame regions near the top and bottom, simulation results are consistent with the two-dimensional observations of Mysels *et al.* (1). Figure 2 shows results for $h(x)$ at two times. The initial shape was taken to be uniform, as in Fig. 1a. More important is h_0, which is large, compared to actual water–soap films, by about a factor of 10. The most important consequence of this is that drainage ($\propto h^3$) is too fast by about a factor of 1000. Thus 1 s in the simulation corresponds perhaps to about 1000 s in the experiments. Characteristic features shown in Fig. 2 are a concave-out profile at early times, indicating significant slip, and an essentially parabolic profile in the middle region at late times, indicating an almost hardened free surface. "Black film" in the figure indicates a thin region near the top that is stabilized by the disjoining contribution to the pressure that has $h \approx h^*$.

The parabolic shape of the late-time profile in Fig. 2 arises simply from the primary balance of viscous and gravitational terms in [2.25] after the free-surface slip velocity u_0 has become vanishingly small. Thus, approximately,

$$h_t = \frac{\rho g}{\mu} h^2 h_x \qquad [3.1]$$

with the kinematic wave solution (1, 32)

$$h = \text{const} \sqrt{\frac{x - x_0}{t}}. \qquad [3.2]$$

At early times, on the other hand, profiles exhibit a characteristic concave-out form. This results from the elongational flow that occurs before surface tension and surface-tension-gradient effects become important. The early-time solution is determined primarily by the simplified evolution equation [2.25a] and a simplified form of the force balance equation [2.24]. These are

$$\frac{Dh}{Dt} \equiv h_t + u_0 h_x = -h u_{0x}, \quad (h u_{0x})_x = -\frac{\rho g}{4\mu} h. \qquad [3.3a, b]$$

Equation [3.3b] may be integrated as

$$h u_{0x} = \frac{\rho g}{4\mu} \int_x^{X(t)} h\,dx, \qquad [3.4]$$

showing that the total tension across the film is simply equal to

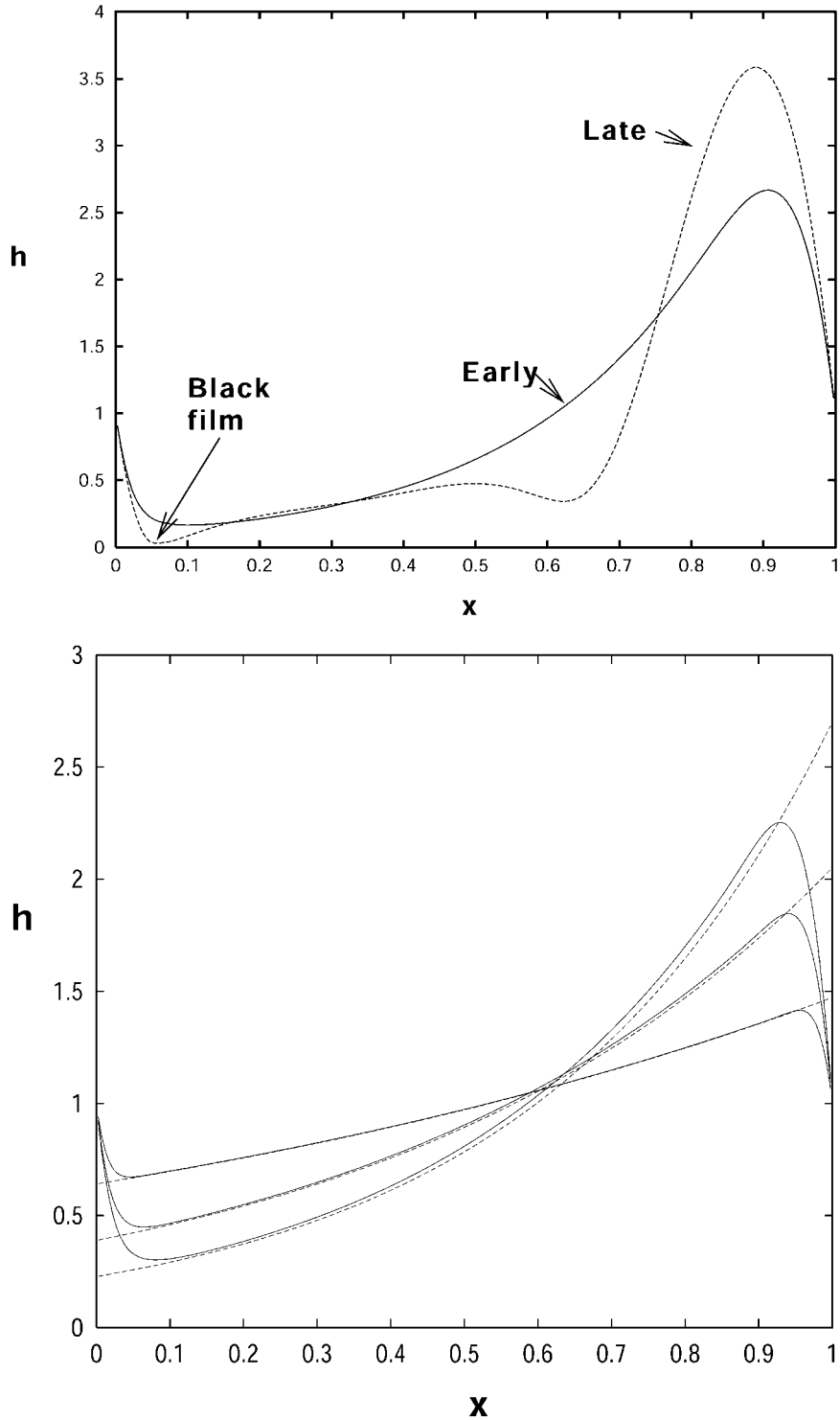

FIG. 2. (Top) Computed dimensionless film profiles at early and late times for an initially uniform film $h(x, 0) = h_0$. Gravity acts in the positive x direction. The early time profile, for dimensionless time $t/T^* = 1.1\ (10^{-6})$, shows a characteristic "hollow ground" shape. The late profile, $t/T^* = 9.0\ (10^{-5})$ shows a "black" film region, followed by a parabolic profile and a growing blob near the bottom support. (Bottom) The same calculation without surfactant. Calculated profiles (solid) are compared with the extensional-flow similarity solution [3.5] (dashed); the times are $t/T^* = 10^{-8}$, 2 (10^{-8}), 3 (10^{-8}).

the "hanging" weight below any station x. The function $X(t)$ depends on the end condition imposed at the lower end of the film. Because the hanging weight and the resulting extensional strain u_{0x} are largest at the top of the film and decrease monotonically with downward distance, the film shape becomes concave-out.

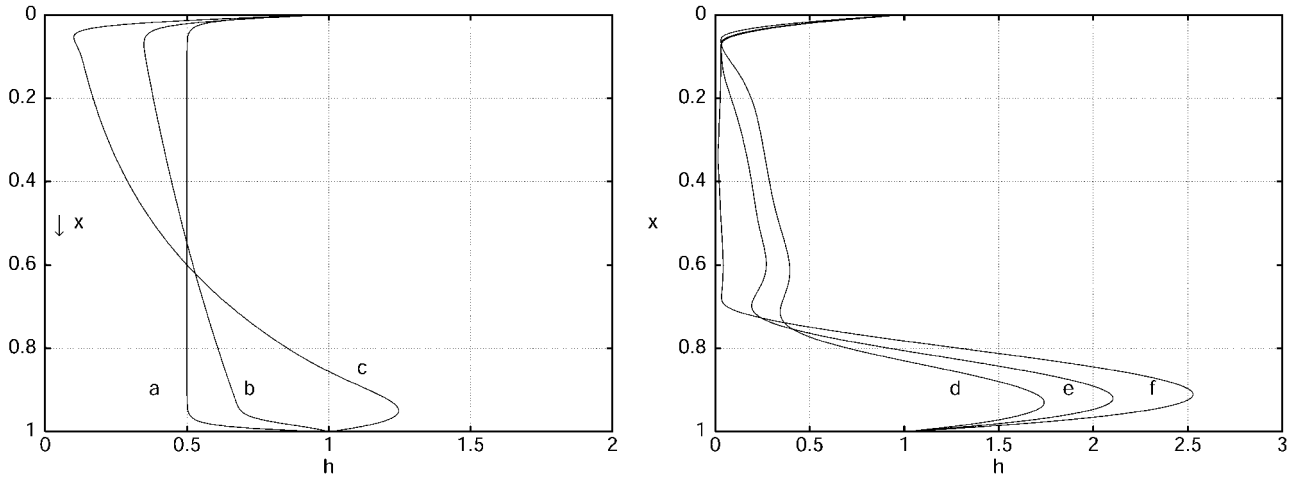

FIG. 3. Draining film profiles at various times for the nominal case with surfactant. See the text for parameter values. The initial profile is thinner in the middle region. (a) $t = 0$, (b) $t/T^* = 10^{-8}$, (c) $t/T^* = 8 \times 10^{-7}$, (d) $t/T^* = 10^{-4}$, (e) $t/T^* = 5 \times 10^{-4}$, (f) $t/T^* = 4 \times 10^{-3}$.

The problem [3.3] is solved by a step-by-step procedure in the Appendix using a Lagrangian description of the motion. (While the solution may easily be verified in the more common Eulerian coordinates, no such deductive procedure appears to be possible in an Eulerian representation.) We show that the evolution of an initially uniform film of thickness h_0 is given by the *similarity solution*

$$\frac{h}{h_0} = f(t)\exp\left(\frac{\rho g t}{4\mu}\, x\right), \qquad [3.5a]$$

where the function $f(t)$ also depends on the lower end condition. The concavity h_{xx} of this exponential curve increases with time t. As shown in the Appendix, for the fixed lower film boundary treated here,

$$f(t) = \frac{kLt}{e^{kLt} - 1}, \quad k \equiv \frac{\rho g}{4\mu}. \qquad [3.5b]$$

Also shown in Fig. 2, the similarity solution [3.5] is compared with a calculation when no surfactant is present. Good agreement can be seen for early times, apart from surface tension "boundary layers" at the top and bottom supports. Note that the characteristic time for the similarity solution $t^* = 4\mu/(\rho g L)$ is equal to $T^*/(B_1 C)$ using the nondimensionalization in [2.28]. Because surface tension effect is not included in the similarity solution, the problem is of lower mathematical order and the end conditions $h(0, t) = h(1, t) = 0$ cannot be satisfied. Comparing the two graphs in Fig. 2 establishes that early-time profile shapes are determined primarily by extensional flow. Comparing the drainage times for the two graphs, however, shows that presence of surfactant slows the drainage significantly before the surfactant has a noticeable effect on the profile shape.

A more complete set of profiles is shown in Figs. 3 to 5. Here the initial shape is not uniform but, apart from connecting exponentials at each end, has an essentially uniform thickness equal to $0.5\, h_0$, which is an arbitrary choice. Because the film is now thinner, drainage takes place more slowly, as expected. In addition to a set of surface shapes at various times, shown in Fig. 3, the corresponding distributions of surfactant are shown in Fig. 4. The characteristic concave-out shape, visible also in Fig. 2, is already apparent at $t/T^* = 8 \times 10^{-7}$. In the intermediate time range from $t/T^* = 10^{-4}$ to 10^{-3}, an almost parabolic profile exists in the middle region with a continually increasing length of black film near the top.

The last profile shown in Fig. 3, at $t/T^* = 0.004$, has the film almost completely drained into a pendant drop shape. As will be seen below, surface tension gradient effect is quite unimportant for this heavy pendant. In fact its shape is almost exactly a balance between surface tension and gravity, satisfying the degenerate steady-state form of [2.29a]

$$h_{xxx} + B_1 = 0. \qquad [3.6]$$

Thus h is a cubic polynomial in x satisfying $h(1) = 1$. In order to find an approximate solution for the static shape, assume all the liquid area is contained in the drop which meets the centerline at zero slope at a point $x = \xi$ to be determined. Thus h is of the form

$$h = 1 + a_1(x - 1) + a_2(x - 1)^2 - B_1\frac{(x - 1)^3}{6}, \qquad [3.7]$$

satisfying the conditions

$$h(\xi) = h_x(\xi) = 0$$

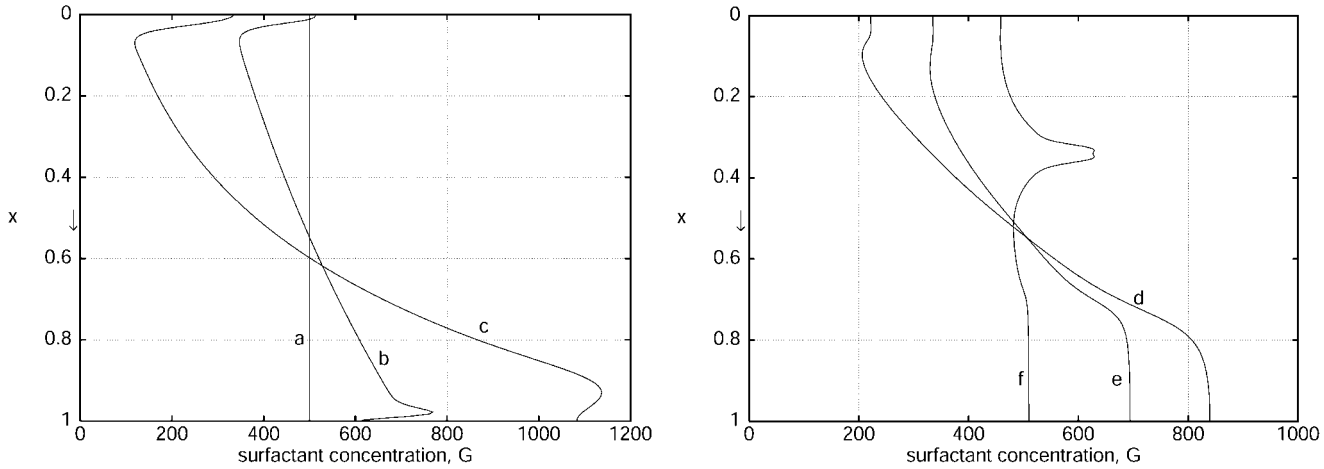

FIG. 4. Surfactant profiles corresponding to the thickness profiles in Fig. 3.

and

$$\int_{\xi}^{1} h dx = A_0,$$

where A_0 is the dimensionless area, equal to 0.510 for the initial profile used here. The complete solution can be shown to be

$$h(x;\,\xi) = (x-\xi)^2\left[\frac{1}{(1-\xi)^2} + \frac{B_1}{6}(1-x)\right], \quad [3.8a]$$

where ξ satisfies the quartic equation

$$\frac{1-\xi}{3} + \frac{B_1}{72}(1-\xi)^4 = A_0. \quad [3.8b]$$

The procedure for finding this solution, in a closely related problem, is given in (33). The pendant profile equation [3.8] closely approximates the final steady-state solution to this problem.

The profiles in Fig. 3 used 200 grid points, and the time step was adjustable so that the maximum change permitted in any h value, per time step, was 3.5×10^{-5}. Run times varied from a few seconds to a few minutes on a Unix Workstation. Had disjoining pressure not been used, the profiles would have been essentially the same until about $t/T^* = 10^{-4}$. At this time, without the disjoining contribution, the thickness begins to decrease rapidly to zero. The simulation fails when h reaches zero anywhere in the computational domain. Unlike the simple pendant rope problem where it was demonstrated mathematically that the thickness falls to zero in finite time (28), it has not been established here that the thickness will reach zero in finite time when Π effects are omitted. Both surface tension and surface tension gradients can support weight; thus the failure that we experience in the model may be either fundamental or purely numerical because the h values must certainly become very small when $\Pi = 0$.

The corresponding surfactant G distribution is shown in Fig. 4. Just as for the h plots of Fig. 3, the x axis is vertical. Initially $G = G_0 = 500$ is uniform. Then, as the surfactant is carried downward by the surface speed U, an upward σ_x traction develops. For this value of G_0, there is sufficient surfactant available to approximately balance the weight in the central region. Note that, in the figure on the right, no G_x is necessary to balance weight in the region near the lower boundary where differences in capillary pressure σh_{xx} support the weight according to Eqs. [3.8a, 3.8b]. As time proceeds, the mid-film thins, its weight decreases and the G_x gradient reduces in magnitude. The last profile shown has a small G_x gradient

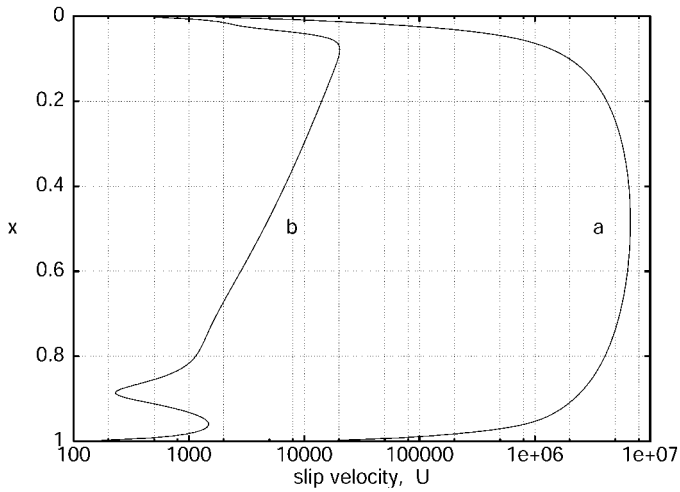

FIG. 5. Semi-log plot of early slip speed profiles for the nominal case. The initial concentration is $G_0 = 500$. Slip speeds at later times are much smaller. (a) $t/T^* = 10^{-8}$, (b) $t/T^* = 8 \times 10^{-7}$.

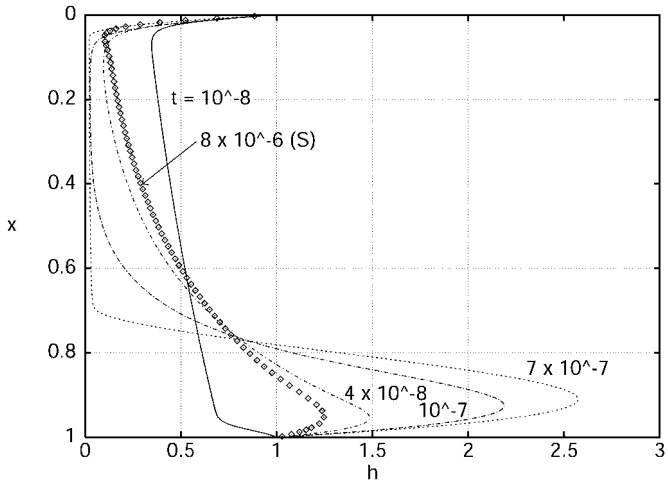

FIG. 6. Profiles without surfactant (lines). Comparison with surfactant (S) with $G_0 = 500$ shown as symbols. The profiles, with and without surfactant, agree at $t/T^* = 10^{-8}$. Disjoining pressure prevents the no-surfactant profiles from going to zero thickness in finite time. The $t/T^* = 7 \times 10^{-7}$ profile has reached steady state and is almost identical to the $t = 4 \times 10^{-3}$ profile with surfactant shown above.

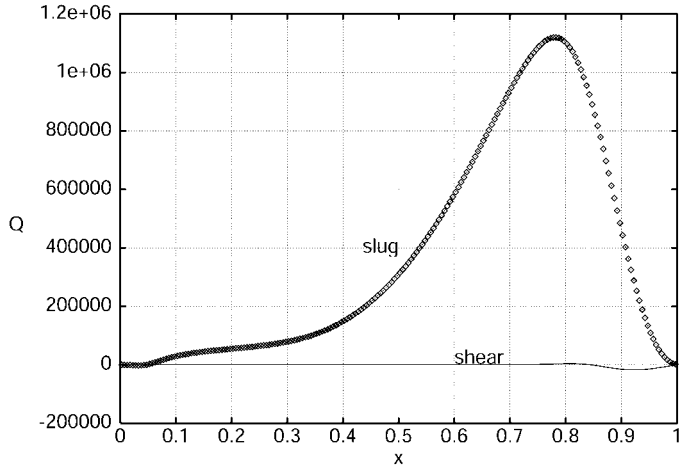

FIG. 7. Slug *Uh* and shear flux components. No surfactant, $t/T^* = 10^{-7}$.

overall since, apart from the pendant blob, the film is thin and requires little weight support. However, note the local peak in G directly over the "blackest" portion of the film. The surfactant is drawn into the thinned portion by the gradient in disjoining pressure. Since, in an improved model, the disjoining forces can be expected to be proportional to local surfactant concentration, this suction effect may be an additional mechanism that helps to prevent film rupture, and, as such, it is potentially important.

Slip velocities are shown in Fig. 5 at two early times. Very early on, for water, the large velocity, when reduced to dimensional form, would correspond to a Reynolds number Re between 100 and 1000. However, had film thicknesses been reduced by a factor of 10 for water, Re would be appropriately small. Other alternatives are to assume liquids of larger viscosity or to take into account the fact that the transition to vertical must happen gradually in an actual experiment, taking perhaps about one second. The high-velocity motion would no longer be present if that were the case.

Figure 6 shows profiles versus time for the same parameter values, except that no surfactant is present; i.e., $G_0 = 0$. The concave-out profiles persist until the static final shape is formed. The motion is quite rapid, perhaps 100 times faster than for the previous surfactant case. Note that the profile at $t/T^* = 10^{-8}$ is virtually identical to the $G_0 = 500$ case, confirming that early deformations, even with surfactant, are virtual slug flows. One other profile with surfactant is shown for comparison.

Flux components for the no-surfactant case are shown in Fig. 7. This figure shows that fluxes come almost entirely from the slug component *Uh* and the shear component has negligible effect. Figure 8, on the other hand, shows flux components with surfactant for $G_0 = 500$. Both components contribute, but the shear flow dominates at $t/T^* = 10^{-4}$.

Figure 9 compares profiles at $t/T^* = 10^{-4}$ with a case where the average surfactant concentration has been increased by a factor of 10 to $G_0 = 5000$. Clearly the rate of drainage has been slowed appreciably. Figure 10 shows that, at this time, the surface is effectively immobile and virtually all the flux arises from a shearing motion that satisfies the no-slip condition on the interface.

Figure 11 considers the nominal-parameter case, but with the length L increased by a factor of 2 to 2 cm. The basic behavior, initial slug fall with concave-out profiles and roughly parabolic shapes at later times, is maintained. The larger pendant drop at the bottom is because the liquid area has been increased. Visible in the figure is a thickness minimum just above the pendant at the latest time. This is the two-dimensional version of a black spot. Black spots are known to form

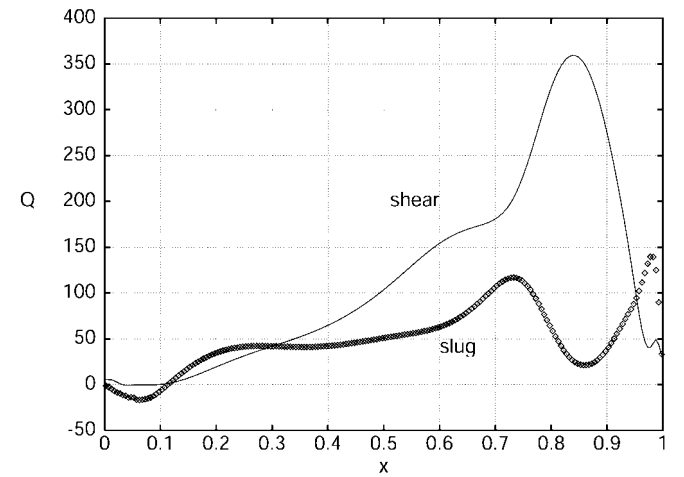

FIG. 8. Slug and shear flux components, $G_0 = 500$, $t/T^* = 10^{-4}$. With surfactant, the shear flow component dominates at this instant in time.

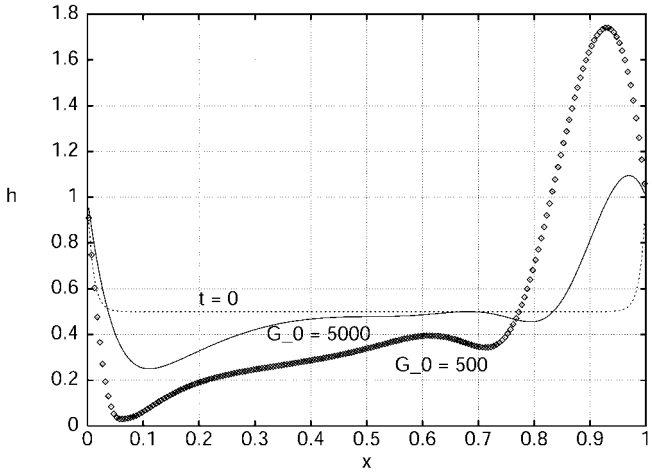

FIG. 9. Film profile comparison at $t/T^* = 10^{-4}$ showing the effect of surfactant. Profiles are shown for $G_0 = 500$ (symbols) and 5000. The initial ($t = 0$) profile is also shown.

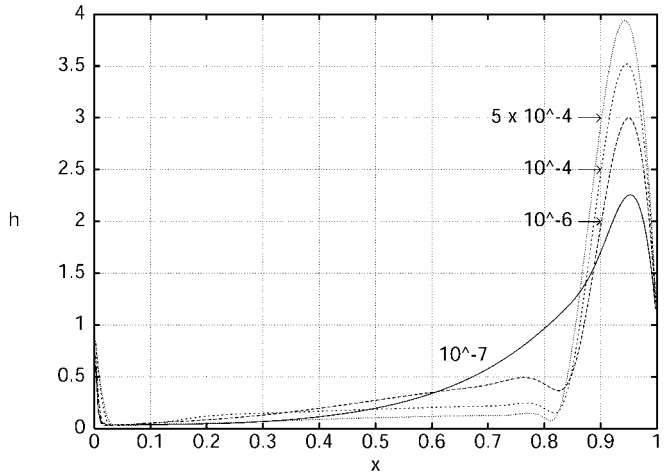

FIG. 11. Profiles at various times for a longer free film, corresponding to $L = 2$ cm. All other physical parameters are the same as for the nominal case. Note that increasing L by a factor of 2 increases the time scale T^* by a factor of 16.

near the bottom of vertical films. This type of local thickness minimum also occurs for drainage flows on solid substrates (34).

4. SUMMARY AND FUTURE MODELING WORK

The theoretical and numerical model for soap film drainage developed in this report reproduces many of the features of this process that have been observed in experiments. These features include the shape of the film thickness profiles and the large differences in draining time scales for low and high surfactant concentrations. When little or no surfactant is present, films drain quickly and assume a concave-out or "hollow-ground" appearance. Conversely, at high concentrations, films quickly "lock in" to an immobile interface mode that is characterized by a downward-opening parabolic shape. This shape drains much more slowly and retains an appreciable thickness for long times. Use of a disjoining contribution in the film pressure allows the simulation of black film. Over a large range of surfactant concentrations, a growing black region forms near the top of the film, in agreement with experiment. For sufficiently long films there is a tendency for black regions to form near the bottom as well. We believe that this is the mechanism leading to the origin of the rising black spots and the associated chaotic motion observed in three-dimensional experiments.

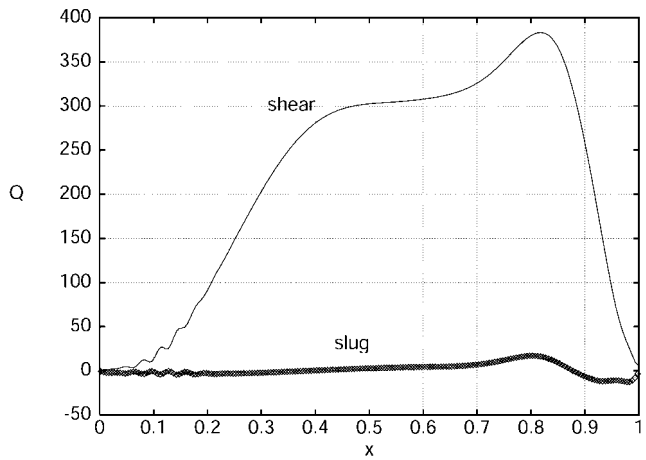

FIG. 10. Slug and shear flux components, $G_0 = 5000$, $t/T^* = 10^{-4}$. The high level of surfactant immobilizes the surface.

A straightforward extension of the present work is a three-dimensional draining simulation that assumes hardened or no-slip interfaces. Within the lubrication approximation, film flow with a hardened surface is equivalent to liquid film flow on a solid substrate. In each case there is one boundary upon which the no-slip condition is applied while the other boundary is a no-shear interface. We have developed numerical schemes for these three-dimensional problems on solid substrates that are immediately applicable to the present problem (35, 19, 20). While far more computationally intensive than two-dimensional simulations, three-dimensional calculations can be made efficient through the use of alternating-direction-implicit or time-splitting numerical algorithms (36–38). With disjoining pressure effects included, "bubble" motions, as well as chaotic motions, can be calculated. Recent soap film experiments have displayed a wide variety of hydrodynamic phenomena, including the generation of vortices and their interactions (39, 40). Wire-frame side wall boundaries conditions, in the simulation, should allow the numerical reproduction of Plateau border suction effects leading to the marginal regeneration observed by Mysels *et al.* (1).

The present model has exploited a number of simplifications in order to focus on the basic mechanisms for this complicated problem. An improved model can examine the processes in more detail. For example, the surfactant has been assumed to be insoluble. While this is a reasonable approximation for

certain surface active substances, a model of more general applicability can consider the details of the diffusional exchange of material between the surface and the bulk liquid film. Such a modification would require the simultaneous solution of additional coupled equations (5, 9). In addition, it is known that a surfactant monolayer has certain properties characteristic of a hypothetical "two-dimensional liquid." One important property in this class is surface shear viscosity (41). Comparison of theoretical results with experimental observation may indicate the need for inclusion of this effect.

The disjoining pressure law used here is only one choice out of a wide class that can be used. Thin stable equilibrium films can be modeled using other choices for the exponents in the law [2.20]. Preliminary tests, using a value $n = 9$ for the repulsive exponent, rather than 4, caused only small changes in the simulation results shown here. More complicated relationships between disjoining pressure and surfactant concentration Γ can also be used. For certain surfactants, a transition from a conjoining or attractive collapse of the film to a disjoining or repulsive force at critical local values of Γ has been reported (6). In any event, it is likely that the intensity of the disjoining effect should reflect the local value of surfactant concentration; that is, one may use $A = A(\Gamma)$ in [2.20].

Other extensions and modifications that can be explored are (i) more general expressions for the surface tension versus surfactant concentration law $\sigma(\Gamma)$, as the linear law used here [2.23] is only valid for small changes in σ, (ii) relaxation of the assumption that the film is bilaterally symmetric, (iii) inclusion of generalized Newtonian rheology for the bulk film flow, and (iv) the incorporation of drying and curing effects. The latter two modifications are of particular importance for nonaqueous films, including those used in the manufacture of dry foam products. Certain of our numerical studies have incorporated simple models for these effects (42, 43).

APPENDIX: DRAINING SOLUTIONS FOR EXTENSIONAL FLOW

We solve the extensional problem [3.3] for various lower end conditions using Lagrangian coordinates. Consider an initially uniform film

$$h(x, 0) = h_0, \quad 0 \le x \le L_0$$

whose evolution is determined by [3.3, 3.4]

$$\frac{Dh}{Dt} = -\frac{\rho g}{4\mu}\int_x^{X(t)} h\,dx. \qquad [A.1]$$

Let ξ be the initial position of a particle in the film that moves to the position x at a later time t, i.e., $x = x(\xi, t)$ and $x(\xi, 0) = \xi$. The the area integral in [A.1] becomes simply

$$\int_x^{X(t)} h\,dx = \int_\xi^{\xi_1(t)} h[x(\xi, 0)]\,d\xi = h_0(\xi_1(t) - \xi) \qquad [A.2]$$

using the initial condition. Here $\xi_1(t)$ is a function that will be determined by the lower-end boundary condition. The derivative following the motion is, in this Lagrangian system,

$$\frac{Dh}{Dt} = \frac{\partial h(\xi, t)}{\partial t}.$$

Also following the motion, the mass-conservation condition is

$$h_0 d\xi = h\,dx, \qquad [A.3]$$

and [A.1] and [A.2] may be combined as

$$\frac{\partial}{\partial t}\left(\frac{\partial \xi}{\partial x}\right) = -\frac{\rho g}{4\mu}(\xi_1(t) - \xi),$$

which integrates to

$$\frac{\partial \xi}{\partial x} = 1 - \frac{\rho g}{4\mu}\left(\int_0^t \xi_1(\tau)\,d\tau - t\xi\right) \qquad [A.4]$$

using $x(\xi, 0) = \xi$. Equation [A.4] is a first-order differential equation for $\xi(x)$, for any fixed t, with the solution

$$\xi(x, t) = g(t)\left[\exp\left(\frac{\rho g t}{4\mu}x\right) - 1\right]$$

for some $g(t)$ after applying the boundary condition $x(\xi = 0, t) = 0$, which expresses the condition that the velocity u_0 is zero at the top of the film. Again using [A.3], the general form of $h(x, t)$ must then be

$$\frac{h}{h_0} = f(t)\exp\left(\frac{\rho g t}{4\mu}x\right) \qquad [3.5a]$$

as given in Section 3.

The solution is completed by specifying the boundary condition at the lower end of the film. The simplest case is a freely falling film of initial length L_0. In this case the suspended weight below a given material element remains constant in time; then $\xi_1 = L_0$ and [3.5a] becomes

$$\frac{h}{h_0} = \left(1 - \frac{\rho g L_0 t}{4\mu}\right)\exp\left(\frac{\rho g t}{4\mu}x\right) \qquad [A.5]$$

as reported in (28). For drainage of a film on a frame with a

fixed lower boundary, as treated in this paper, the no-flow condition is $u_0\ (x = L_0) = 0$. A general expression for the speed variation can be obtained from the profile equation [3.5a],

$$u_0(x, t) = -\frac{1}{h}\int_0^x h_t(\eta, t)d\eta = \frac{1 - e^{-ktx}}{kt}\left(\frac{1}{t} - \frac{1}{f}\frac{df}{dt}\right) - \frac{x}{t}, \qquad [A.6]$$

where $k = \rho g/(4\mu)$. The condition $u_0(L_0, t) = 0$ provides a quadrature formula for $f(t)$ subject to $f(0) = 1$. A closed-form expression for f can be found, and the similarity solution is

$$\frac{h}{h_0} = \left(\frac{kL_0t}{e^{kL_0t} - 1}\right)e^{ktx}. \qquad [A.7]$$

This may be approximated, using a Taylor series for $kL_0t \ll 1$, by

$$\frac{h}{h_0} \approx \exp\left[\frac{\rho g t}{4\mu}\left(x - \frac{L_0}{2}\right)\right].$$

This approximation is seen to be a growing exponential "horn" with a fixed node at the film midpoint.

The experiment setup of Mysels *et al.* (1), where the soap film is allowed to drain into a bath, is more closely approximated by using the boundary condition $u_{0x}(L_0, t) = 0$. With $x = L_0$ representing the level of the bath, the extensional stress or film tension is approximately zero there. A closed-form expression for $f(t)$ can be found for that case as well. The similarity solution is

$$\frac{h}{h_0} = \frac{kL_0t}{\exp[C + Ei(kL_0t)]}\,e^{ktx}, \qquad [A.8]$$

where C is Euler's constant and Ei is the Exponential-integral function (44). For small times, [A.8] is approximated by

$$\frac{h}{h_0} \approx \exp\left[\frac{\rho g t}{4\mu}\,(x - L_0)\right],$$

which shows an invariant node at the level of the bath. Note that the similarity solution for the hanging rope problem [A.5] predicts that the film thickness will fall to zero in finite time. For the other two cases, film thicknesses only approach zero asymptotically as $t \to \infty$.

ACKNOWLEDGMENTS

This work is supported by the NASA Microgravity Program, the ICI Business Link Partnership, and the State of Delaware.

REFERENCES

1. Mysels, K., Shinoda, K., and Frankel, S., "Soap Films, Studies of their Thinning." Pergamon, New York, 1959.
2. Newton, I., "Opticks." Smith and Walford, London, 1704.
3. Wilson, A. J., Ed., "Foams: Physics, Chemistry and Structure." Springer-Verlag, London, 1989.
4. Woods, G., "The ICI Polyurethanes Book." ICI Polyurethanes/Wiley, Chichester/New York, 1990.
5. Jensen, O. E., and Grotberg, J. B., *Phys. Fluids A* **5,** 58 (1993).
6. Bhakta, A., and Ruckenstein, E., *Adv. Colloid Interface Sci.* **70,** 1 (1997).
7. Weaire, D., Hutzler, S., Verbist, G., and Peters, E., *Adv. Chem. Phys.* **102,** 315 (1997).
8. Schwartz, L. W., and Princen, H. M., *J. Colloid Interface Sci.* **118,** 201 (1987).
9. Levich, V. G., "Physiochemical Hydrodynamics." Prentice Hall, Englewood Cliffs, NJ, 1962.
10. Schwartz, L. W., Weidner, D. E., and Eley, R. R., *Langmuir* **11,** 3690 (1995).
11. Schwartz, L. W., Cairncross, R. A., and Weidner, D. E., *Phys. Fluids* **8,** 1693 (1996).
12. Frumkin, A. N., *Zh. Fiz. Khim.* **12,** 337 (1938).
13. Derjaguin, B. V., *Zh. Fiz. Khim.* **14,** 137 (1940).
14. Churaev, N. V., and Sobolev, V. D., *Adv. Colloid Interface Sci.* **61,** 1 (1995).
15. Williams, M. B., and Davis, S. H., *J. Colloid Interface Sci.* **90,** 220 (1982).
16. Teletzke, G., Davis, H. T., and Scriven, L. E., *Chem. Eng. Commun.* **55,** 41 (1987).
17. Kheshgi, H. S., and Scriven, L. E., *Chem. Eng. Sci.* **46,** 519 (1991).
18. Mitlin, V. S., *J. Colloid Interface Sci.* **156,** 491 (1993).
19. Schwartz, L. W., and Eley, R. R., *J. Colloid Interface Sci.* **202,** 173 (1998).
20. Schwartz, L. W., *Langmuir* **14,** 3440 (1998).
21. Schwartz, L. W., *in* "Free-Surface Flows with Viscosity" (P. Tyvand, Ed.), pp. 203–233. Computational Mech. Publ., Southampton, 1997.
22. Erneux, T., and Davis, S. H., *Phys. Fluids* **A5,** 1117 (1993).
23. De Wit, A., Gallez, D., and Christov, C. I., *Phys. Fluids* **6,** 3256 (1994).
24. Breward, C., Darton, R., Howell, P., and Ockendon, J., "Modelling Foam Drainage," I. Chem. E. Symp. Series No. 142(2), pp. 1009–1019, undated.
25. Ramos de Souza, E., and Gallez, D., *Phys. Fluids* **10,** 1804 (1998).
26. Eggleton, C. D., and Stebe, K. J., *J. Colloid Interface Sci.*, 1999.
27. Trouton, F. T., *Proc. Roy. Soc. A* **77,** 426 (1906).
28. Stokes, Y., Tuck, E. O., and Schwartz, L. W., submitted.
29. Chang, H-C., *Annu. Rev. Fluid Mech.* **26,** 103 (1994).
30. Stoyanov, S. D., Paunov, V. N., Basheva, E. S., Ivanov, I. B., Mehreteab, A., and Broze, G., *Langmuir* **13,** 1400–1407.
31. Braun, R. J., Snow, S. A., and Pernisz, U. C., submitted.
32. Moriarty, J. A., Schwartz, L. W., and Tuck, E. O., *Phys. Fluids A* **3,** 733 (1991).
33. Tuck, E. O., and Schwartz, L. W., *J. Fluid Mech.* **223,** 313 (1991).
34. Wilson, S. D. R., and Jones, A. F., *J. Fluid Mech.* **128,** 219 (1983).
35. Weidner, D. E., Schwartz, L. W., and Eres, M. H., *J. Colloid Interface Sci.* **187,** 243 (1997).
36. Peaceman, D. W., and Rachford, H. H., *SIAM J.* **3,** 28 (1955).
37. Yanenko, N. N., The Method of Fractional Steps." Springer-Verlag, New York, 1971.
38. Conte, S. D., and Dames, R. T., *Math. Tables Aids Comput.* **12,** 198 (1958).
39. Couder, Y., Chomaz, J. M., and Rabaud, M., *Physica D* **37,** 384 (1989).
40. Goldburg, W. I., Belmonte, A., Wu, X. L., and Zusman, I., *Physica A* **254,** 231–247 (1998).
41. Edwards, D. A., Brenner, H., and Wasan, D. T., "Interfacial Transport Processes and Rheology." Butterworth–Heinemann, Boston, 1991.
42. Weidner, D. E., Schwartz, L. W., and Eley, R. R., *J. Colloid Interface Sci.* **179,** 66 (1996).
43. Eres, M. H., Weidner, D. E., and Schwartz, L. W., *Langmuir* **15,** 1859 (1999).
44. Gradsteyn, I. S., and Rhyzhik, I. M., "Table of Integrals, Series, and Products." Academic Press, New York, 1965.